# Aspects of Phasor Angle Measurement for Wind Farm Protection Applications

Nagy I. Elkalashy, Tamer A. Kawady and Naema M. Mansour

*Abstract*--**Real time measurement of phasor angle is nowadays required in modern power system purposes. For protection applications of large grid-integrated wind farms, in particular, accurate estimation of current angles may be utilized for fault analysis, detection and location purposes. Severe transients, AC amplitude decaying and significant DC-decay offset of fault current contributed by the induction generators may significantly affect the accuracy of real time phasor estimation procedures. Those aspects are broadly investigated in this paper. Different mathematical cores including Discrete Fourier Transform (DFT), Kalman filtering and Least Squared (LS) computational methods are considered in this study. Fault cases are taken from a typical wind farm simulation with Matlab package. The results provide a better understanding of the digital phasor extractor performance in the real field.**

*Keywords*: **keywords. Wind Farm Protection, DFT, Kalman Filtering, Least Squared error.**

## I. INTRODUCTION

THE impressive growth in the utilization of wind energy has consequently spawned promising research activities in a wide variety of technical fields. Moreover, the increasing penetration of wind energy into conventional power systems highlights several important issues such as reliability, security, stability, power quality and protection applications.

Among the abovementioned issues, providing wind farms with the proper protection is quite essential. The essential benefits from the dedicated protection functions are to avoid the possible local damage resulting from incident faults and minimize the impact of these abnormal conditions on other sound parts of the network. This consequently enhances the reliability and dependability of the overall grid performance.

Wind farms are characterized with some unique features during their normal and faulty operating conditions. Different factors participate usually into these conditions such as the distributed generation concept, the own behavior of the wind generator and varying wind speed. Moreover, the dynamic behavior of the wind generators during disturbances depends mainly on their type and their associated control strategies [1]. The common type of the wind turbine generators that are commercially available nowadays are permanent magnet synchronous generator (PMSG) and induction generator (IG). The latter are the most preferable generator type nowadays for driving wind turbines due to the uncontrollable characteristic of wind speed.

During faults in wind farms, high DC-decay offset is observed in the fault current due to the dynamic response of the IGs accompanied with their time varying parameters. AC amplitude decaying is remarked as well [2]. Under such circumstances, there is a challenge to accurately identify the fault current direction using the phasor angles. The current direction can be utilized to estimate the faulty zone without real communication channels, if it is accurately estimated.

Digital signal processing is widely applied in digital relays in order to extract the fundamental phasors for protection applications such as fault classification, overcurrent protection, distance protection, differential protection, ground fault detection and fault location. Among the most famous algorithms for such purposes, DFT [3], [4], Kalman [5]-[8] and Least square (LS) [9]-[11] arise as the most common ones. In the literatures, such algorithms are evaluated in order to overcome the DC-decaying component in the fault current. However, the performance with AC amplitude decaying is not assessed sufficient till present.

The objective of this paper is to evaluate the performance of DFT, Kalman and LS for phasor extraction of fault currents in wind farms. A practical example of Egyptian wind farm is simulated in the Matlab package. This simulation is used to take fault cases. Then, their phasors are extracted using the aforementioned mathematical methods. For reasonable comparison between them, the extracted phasors of known digital signals are evaluated where this signal is designed to contain AC amplitude decaying and DC-decay offset.

## II. WIND FARM CONSTRUCTION AND PROTECTION OVERVIEW

### A. Wind farm Construction

Fig. 1 shows a schematic diagram of a typical wind farm. Nowadays, modern wind farms include 20 to 150 units with typical size up-to 5 MW wind turbine-generator sets. Larger rates with 7 and 10 MW will be available soon in the market. The typical generator's terminal voltage may range from 575 to 690 V with frequency of 50/60 Hz. The generator terminal voltage is stepped up to the "Collector Bus" system with typical voltage ranged from 22 to 34 kV. The step up transformer is an oil cooled, pad mounted located at the base of the wind turbine unit. Sometimes, the step up transformer is mounted in the turbine nacelle (with dry ones). Certain considerations should be applied for avoiding the harmonic
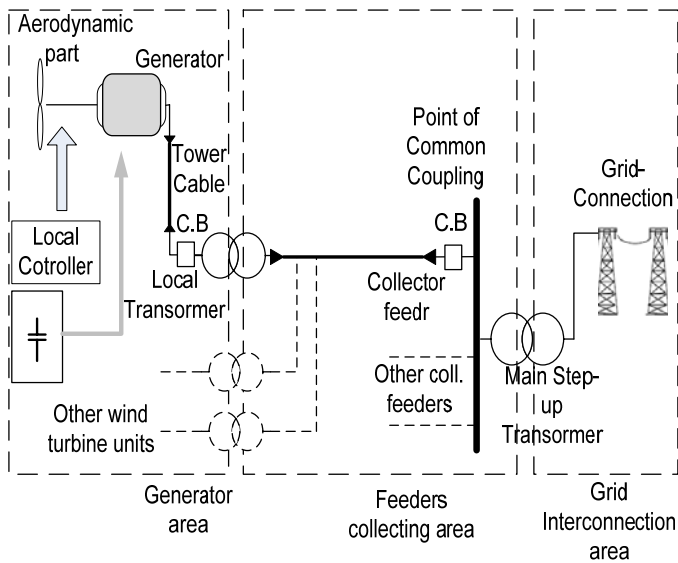
Fig. 1 Typical wind farm construction with its protection zones.

effects. Usually some reactive power compensation units are provided by a collection of switched capacitors. Finally, the collected power is transferred to the utility side via an interconnection step up transformer [1].

The two basic types of wind turbines used nowadays are Fixed-Speed Wind Turbine (FSWT) and Variable-Speed Wind Turbine (VSWT). Squirrel-cage induction generators work normally within a limited wind speed range, which is one of their main drawbacks in comparison with variable-speed ones. Variable-speed wind turbines are mainly equipped with a doubly-fed induction generators (DFIG) with variable frequency excitation of the rotor circuit. The stator windings are connected directly to the AC grid whereas the rotor windings are coupled through a partial scale back-to-back converter. The main advantage of DFIG wind turbines is their ability to supply power at a constant voltage and frequency while variations of the rotor speed. The concept of DFIG for variable-speed wind turbine provides the possibility of controlling the active and reactive power, which is a significant advantage regarding grid integration.

### B. Wind farm Protection

The wind farm protection system is usually divided into different protection zones including the wind farm area, wind farm collection system, wind farm interconnection system and the utility area. First, the induction generator protection is typically accomplished via the generator controlling system covering some certain protection functions such as under/over voltage, under/over frequency, and generator winding temperature (RTDs). Whereas, the generator control system does not contribute for the interconnecting system or the utility zone [1].

The generator step up transformer is usually protected with primary fuses. For those cases when the transformer is mounted in the nacelle, a circuit breaker is integrated with dedicated phase and ground time-overcurrent relays. The collector feeder protection is simplified considering it as a radial distribution feeder using overcurrent protection (50/51).

A basic challenge arises due to the distributed generators connected together to the radial feeder in determining the minimum faulty zone. That is in order to keep the remaining sound parts of the farm supplying the power. On the other hand, the protection of the wind farm substation collector bus and main power transformer consists of multi-function numerical relay system including main transformer differential relay, transformer backup overcurrent relay, collector bus differential relay and breaker failure relay [12]-[15].

Considering the utility area, different protection functions may be used according to the voltage level and the considered protection topology. Direct transfer trip scheme, line differential relay, pilot protection, zones distance relaying, over/under voltage protection, over/under frequency protection, breaker failure protection, synchronous checking and backup overcurrent protection can be used [1]. Communication system with dedicated SCADA is quite important for wind farm operation. Nowadays, the data from each wind generator control is transmitted via optic cables and spread the substations for general control and monitoring purposes. This provides an ideal situation for providing them with an integrated monitoring and protection system.

Owing to the *distributed generation* topology (where the utilized generation sets share a typical radial distribution feeder), such networks raise their particular fault current contribution. During normal power flow, the accumulated current is incremented regularly towards the common coupling point. Faults, on the other hand, disturb the normal current distribution forcing the flowing currents beyond the fault point to reverse their direction towards the fault point. Then, sensing the fault current direction can be therefore utilized to pinpoint the faulty segment along the faulty feeder. For achieving this goal, realizing a dependable and accurate phasor estimation computation may be essential.

### III. MODELING ISSUES

#### A. Egyptian Wind Farm

A 425 MW wind farm was established in Al- Zaafarana, 220 south east of Cairo, Egypt and connected to the 220 kV Egyptian grid. This promising area is distinctive with different superior features such as an average annual wind speed of 9.5 m/s, and its excellent geographical and environmental features. The farm was structured through seven stages of 30, 33, 30, 47, 85, 120 and 80 MW respectively. Except the latter three stages, other ones are with fixed speed and variable pitch operation. Currently, two further stages are being constructed adding extra 240 MW to the farm. The fifth stage is selected for the simulation purposes representing a typical example for variable speed operations. The fifth stage consists of 100 wind turbines (with a 850 KW DFIG units for each turbine) providing a total power of 85MW. Fig. 2 demonstrates the distribution of the turbine units with seven collecting feeders for the considered stage showing the number of utilized turbine units for each feeder. Each wind turbine-generator was represented explicitly in the simulation using Simulink/Matlab with its full dynamic DFIG model.
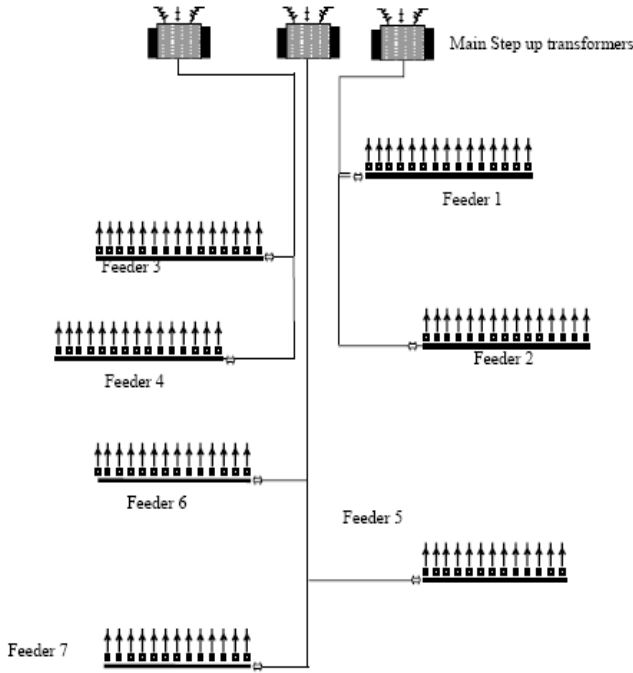
Fig. 2 Schematic of fifth stage of Al-Zaafarana wind farm.

Each wind turbine is connected to a 690V/22 KV local step-up transformer and then integrated with the grid through 22/220 kV step-up transformers. The collecting feeder (7) was considered for developing the required simulation examples for this study.

When a 3-phase fault occurs, the crowbar will short circuit the IG rotor circuit to protect the inverter against over-voltage. When the crowbar circulatory is fired, the DFIG will act as a squirrel cage IG which excitation is dependent on the grid. The nominal wind speed was assigned to 9.5 m/sec (according to the annual average wind speed in its corresponding location), whereas the "cut-in" speed was assigned to be 4.5 m/sec. Further details for the utilized simulation platform are available in [16].

### B. Problem Clarification

Fig. 3 described the collector feeder current supported by one of the generators and feeding for a three-phase fault case occurred at the point of common coupling along feeder (7) of the simulated fifth stage of Al-Zafarana farm. Turbines along feeders 5, 6, and 7 are the sole contributors for the fault current. After the fault occurrence, the DC-decay offset is positive in phase-a and negative in phase-b while there is no offset in phase-c. The other observation is that the AC amplitude is decaying as very clear in phase-c.

For unsymmetrical faults, the transient behaviour of d-q models representing electrical machines has not been sufficiently verified up to now in almost all electromagnetic programs. On the other hand, the performance of such d-q representations for three phase faults was justified well. Hence, considering three-phase fault is preferred for investigating phasor measurements in a simulated network including AC machines such as the example under study.
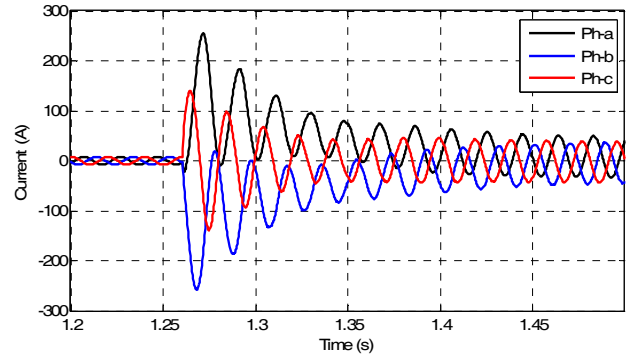


Fig. 3. The collector feeder current for three-phase fault occurred at the point of common coupling at 1.260 s.

Furthermore, the three-phase fault can provide +ve, zero and −ve dc decaying in the fault current which considers various dc decaying and may represent the worst conditions for phasor measurements.

## IV. DIGITAL PHASOR EXTRACTOR CORES

In this section, three approaches are evaluated for extracting the phasors of the current waveforms shown in Fig. 3. They are DFT, Kalman and LS as discussed in following.

### A. DFT Computational Routine

Towards reducing the Fourier Transform computational time, Fast Foureier Fransform (FFT) has been used. However, the FFT pitfalls can be summarized as follows [17-18]. The aliasing is alleviated by satisfying that the sampling frequency must be greater than twice the highest frequency in the signal to be analyzed. The leakage effect is avoided, when the number of samples per cycle period of resolution frequency is an integer. However, the picket fence effects are produced if the waveform has frequencies are not integer multiples of resolution frequency. Last condition is that waveforms must be stationary and periodic.

Concerning the DFT algorithm for the phasor identification it is important to underline that several algorithms have been proposed. In particular, DFT-based algorithms can be grouped into one-cycle DFT estimators, and fractional-cycle DFT estimators performing recursive and non-recursive updates [19-20]. The coefficients of Fourier Transforms are determined by the inner product of input function being transformed and one of the bases functions that are sines and cosines of different frequencies. The voltage and current phasors are tracked using a recursive Discrete Fourier Transform (DFT). The recursive DFT is in the form [3]:

$$X_{real} = X_{real} + 2(x(k) - x(k-N))\sin(k\theta)/N \quad (1)$$

$$X_{imag} = X_{imag} + 2(x(k) - x(k-N))\cos(k\theta)/N \quad (2)$$

$$X = X_{real} + iX_{imag} \quad (3)$$

where $x(.)$ is the discrete input samples of the voltage or current at sample number $k$. $X_{real}$, $X_{imag}$ and $X$ are the in-phase, quadrature-phase and the phasor in complex, respectively. $N$ is the number of samples per the power cycle and $\theta = 2\pi/N$.
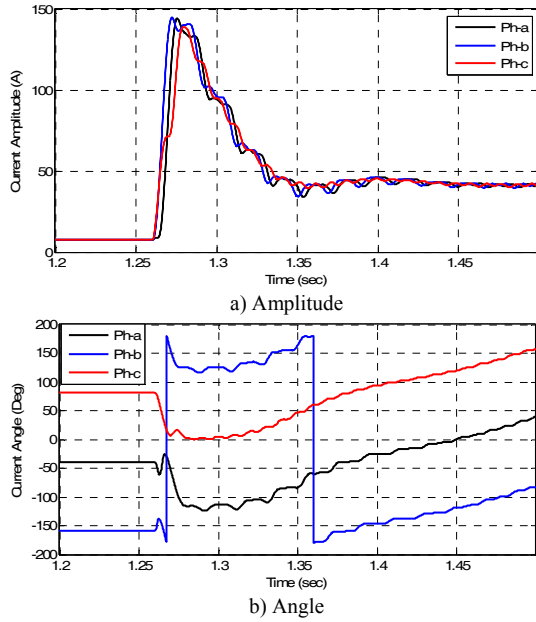
a) Amplitude



b) Angle

Fig. 4 DFT Performance for extracting phasors of the current waveforms shown in Fig. 3.



a) Amplitude



b) Angle

Fig. 5  Kalman Performance for extracting the current phasors.

Fig. 4 shows the performance of the recursive DFT when it is used for extracting the current waveforms shown in Fig. 3. The DFT apparently succeeded to track the current amplitude and angle changes. However, it is difficult to calculate the phasor estimation error extracted by the DFT using the waveforms from a detailed dynamic simulation.

*B.  Kalman Computational Routine*

In [5], Kalman filter is used for timely tracking of phasors of power system voltage and current waveforms and their harmonics. The Kalman filter is based on a state space approach, in which a state equation models the dynamics of the signal process and an observation (measurement) equation models the noisy observation signal. If input signal $x(t)$ has amplitude $A$, frequency $\omega_0$, phase shift $\theta$ and dc decaying of $B$ amplitude and $\tau$ time constant, it can be written as:

$$x(t) = A\sin(\omega t + \theta) + Be^{-t/\tau}$$

$$= x_1 \cos(\omega t) + x_2 \sin(\omega t) + x_3 e^{-t/\tau} \qquad (4)$$

where $x_1 = A\sin(\theta)$, $x_2 = A\cos(\theta)$ and $x_3 = B$. It can be described in the following state equations:

$$x_{k+1} = \phi_k x_k + w_k$$

$$\begin{bmatrix} x_1 \\ x_2 \\ x_3 \end{bmatrix}_{k+1} = \begin{bmatrix} 1 & 0 & 0 \\ 0 & 1 & 0 \\ 0 & 0 & 1 \end{bmatrix} \begin{bmatrix} x_1 \\ x_2 \\ x_3 \end{bmatrix}_k + \begin{bmatrix} w_1 \\ w_2 \\ w_3 \end{bmatrix}_k \qquad (5)$$

where $w_k$ allows the state variables to random walk (time variation). The measurement equation would include the signal and noise and it can be represented as:
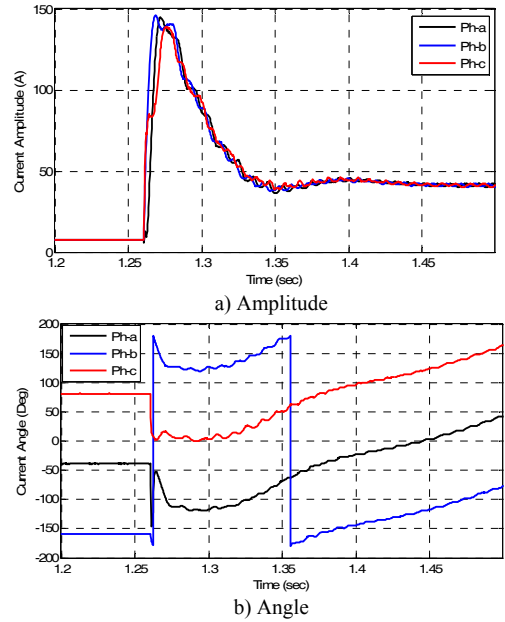
$$Z_k = \begin{bmatrix} \cos(\omega t_k) & \sin(\omega t_k) & e^{-t_k/\tau} \end{bmatrix} \begin{bmatrix} x_1 \\ x_2 \\ x_3 \end{bmatrix}_k + v_k \qquad (6)$$

where $v_k$ represents the error due to noise or un-modeled harmonics. However, this Kalman derivation is only suitable for input signal defined in eqn. (4) and therefore presented in the state eqn. (5) and in the measurement eqn. (6). For on-line application of Kalman approach, the aforementioned state equations are solved using the steps mentioned in [5]-[8]. The prediction of state is based on the samples available up to time $k$ and it can be expressed recursively as a linear combination of the prediction based on the samples available up to time $k-1$ and innovation signal at time $k$. Not only describing the state space equations but also selecting Kalman parameters is a challenge for its accurate applications; for example, initial process vector, noise variance and state variable covariance matrix. In the current study, the default values for the Kalman applications in power system transients are considered as reported in [5].

By applying the Kalman algorithm on the current waveforms shown in Fig. 3, the corresponding performance is shown in Fig. 5. The Kalman performance is apparently similar to the DFT performance shown previously in Fig. 4.

*C.  LS Computational Routine*

Utilizing "Least Square Technique" (LS) for estimating electrical phasors is based on curve fitting of the collected trail of measured samples that are captured at evenly distributed points in time over certain time window. As compared with orthogonal algorithms, LS is distinctive with their ability to reproduce the unknown decaying parameters in conjunction with the periodical harmonic contents. Considering *n*

harmonic orders, the unknown time samples can be described as a function of time as;

$$e(t) = K_1 e^{-t/\tau} + K_2 \sin(\omega_0 t + \theta_1) + \ldots + K_n \sin(n\omega_0 t + \theta_n) \quad (7)$$

Using Taylor's series, the exponential part $(e^{-t/\tau})$ can be expressed as,

$$e^{-t/\tau} = 1 - \frac{t}{\tau} + \frac{1}{2!}\frac{t^2}{\tau^2} - \ldots\ldots\ldots\ldots \quad (8)$$

Considering only the first three terms of the taylor' terms, Eqn. (7) can be rewritten as,

$$e(t) = K_1 - K_1\frac{t}{\tau} + K_1\frac{1}{2!}\frac{t^2}{\tau^2} + K_2\sin(\omega_0 t + \theta_1) + \ldots + K_n\sin(n\omega_0 t + \theta_n) \quad (9)$$

For a predetermined window length with $m$ known samples, the related signal can be then profiled as,

$$\begin{bmatrix} a_{11} & a_{12} & \ldots & a_{1(2n+3)} \\ a_{21} & a_{22} & \ldots & \ldots \\ \ldots & \ldots & \ldots & \ldots \\ a_{m1} & \ldots & \ldots & a_{m(2n+3)} \end{bmatrix} \begin{bmatrix} x_1 \\ x_2 \\ \ldots \\ x_{2n+3} \end{bmatrix} = \begin{bmatrix} e(t_1) \\ e(t_2) \\ \ldots \\ e(t_m) \end{bmatrix} \quad (10)$$

where $a_{11}$, $a_{22}$, ….. are computed according to the known constants from eqn. (9), whereas $x_1$, $x_2$, … are the unknowns required to be estimated. Then the unknown vector $[x]$ can be directly computed each sample as:

$$[x] = ([a^t][a])^{-1}[a][e] \quad (11)$$

These resulting estimated unknowns can be then employed to calculate the corresponding magnitudes and angles of the selected harmonics in addition to the accompanied DC component.

Fig. 6 shows the LS performance when it is used for tracking the current waveforms shown in Fig. 3. The LS performance is apparently similar to the DFT shown in Fig. 4 and to the Kalman shown in Fig. 5.

For the comparison point of view, Fig. 7 shows the performance of the three approaches considering phase-a only. There is a small difference between their performances. However, it is difficult to decide which approach is the most accurate one. To give an answer, the parameters of the input signal should be known as discussed in the following section.

## V. EXTRACTOR PERFORMANCE EVALUATION USING STATIC INPUT SIGNAL

A static input signal is designed in order to evaluate the performance of DFT, Kalman and LS. It is observed after the fault instant in the waveforms shown in Fig 3 that there is DC-decay offset and decaying in the AC amplitude. Therefore, the designed waveform can be in the form:

$$x(t) = \begin{cases} A_1 \sin(\omega t + \theta_1) & \text{for } t < t_f \\ (A_2 + A_3 e^{-t/\tau_1})\sin(\omega t + \theta_2) + A_4 e^{-t/\tau_2} & \text{for } t > t_f \end{cases} \quad (12)$$
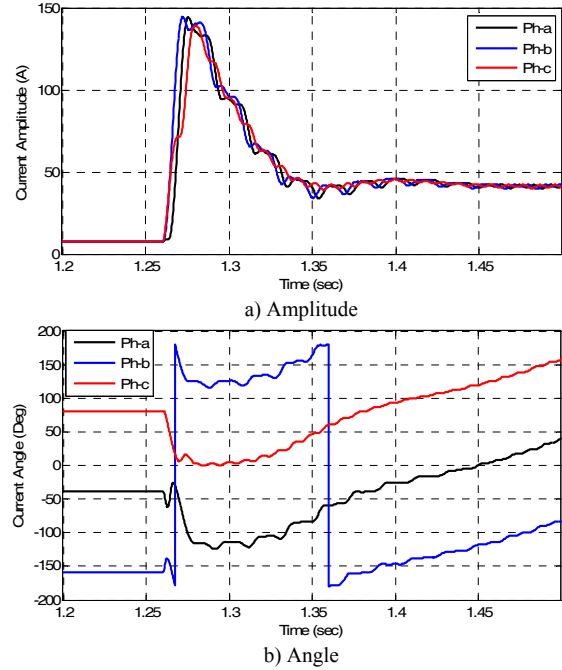


a) Amplitude



b) Angle

Fig. 6 LS Performance for extracting the current phasors.
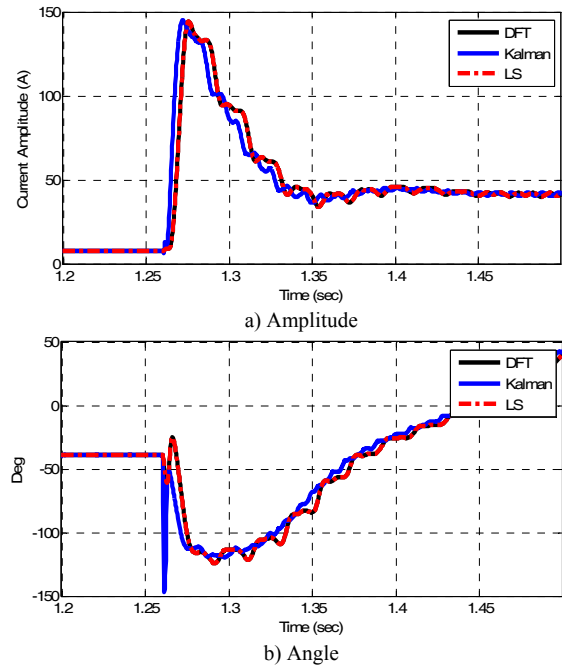


a) Amplitude



b) Angle

Fig. 7 Comparing the performance of the selected algorithms considering phase-a current waveform.

In this signal, the reference amplitude is changed from $A_1$ to $(A_2 + A_3 e^{-t/\tau_1})$ at the instant $t_f$ while the angle is changed from $\theta_1$ to $\theta_2$. After this instant $t_f$, there is DC offset decay with amplitude $A_4$ and time constant $\tau_2$. Fig. 8 shows the performance of the DFT, Kalman and LS considering an assumption that the static signal parameters are $A_1 = 50$, $A_2 = 100$, $A_3 = 250$, $A_4 = 200$, $\theta_1 = -3\pi/4$, $\theta_2 = \pi/4$, $\tau_1 = 0.020$ and $\tau_2 = 0.080$. By comparing the performance with respect to the reference amplitude and reference angle, the Kalman algorithm is the best one where it is close to the reference
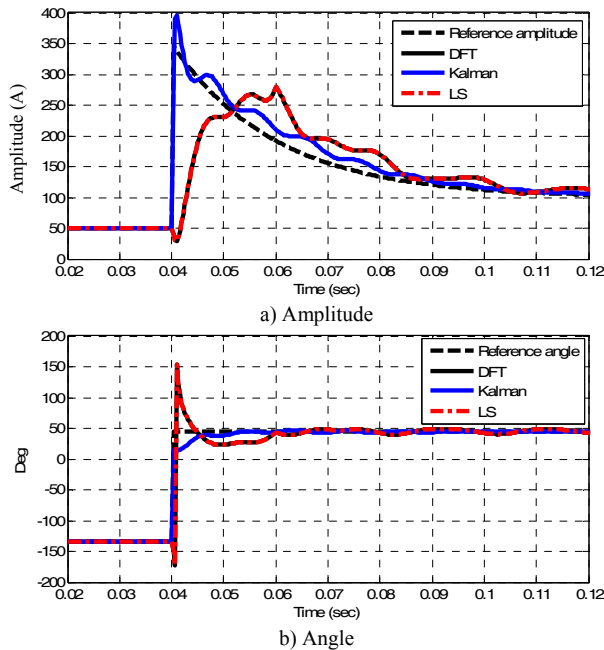
a) Amplitude



b) Angle

Fig. 8   Comparing the performance of the selected algorithms considering known reference.

amplitude and the reference angle within half cycle from the disturbance instant. After this half cycle, the Kalman performance is still better than the others.   The prediction behavior of Kalman filter provides better performance to quickly track the signal transient. So, Kalman correctly define the change within half-cycle. Including the time constant parameter in Kalman derivation (as in Eqns. (4) to (6)) gives the ability to overcome the effect of dc decaying on the phasor extraction.

## VI. CONCLUSIONS

During faults in wind farms, the fault current features are suddenly increased with high DC offset decay and AC amplitude decay. Such features provide errors during extracting the current phasors. Three algorithms of DFT, Kalman and LS have been evaluated for the phasor extraction of current waveforms captured from a well prepared fault cases from a detailed dynamic simulation of a real wind farm. A 425 MW wind farm in Al-Zafarana-Egypt has been considered as a simulated example. Apparently, the three algorithms succeeded to extract the phasors. For deciding which algorithm provides better performance, a static signal input has been designed. The Kalman performance has been found better than the DFT and LS. However, the computational time in real time of each algorithm has been not evaluated yet. This will be experimentally done using DSP boards in a work to follow.

## VII. APPENDIX

The data of the wind farm is as following.
- Nominal wind speed 9.5 m/s, cut-in wind speed 5.4 m/s
- 3 blades with diameter 58 m, swept area 2642.08 m² and rotor speed rating range 14.06-30.08 rpm.
- DFIG Generator: 850 kW Asynchronous rated 690 V with speed range 900-1900 rpm.
- Transformers: Farm transformer rating 0.69/22 kV, 5%, Delta/Star earthed while the grid transformer 22/220 kV, 0.16, Delta/Star earthed.
- Feeder parameters: + ve and zero sequence resistances 0.1153 and 0.413 Ω/km, respectively. +ve and zero sequence inductances are 1.05 and 3.32 mH/km, respectively. + ve and zero sequence capacitances 11.33e-009 5.01 nF/km, respectively.

## IX. REFERENCES

[1] Tamer Kawady, Naema Mansour and A. I. Taalab, "Wind Farm Protection Systems: State of the Art and Challenges", a book chapter in "Alternative Energy", edited by D. N. Gaonkar, ISBN 978-953-307-046-9, Intechweb, Vienna, Austria, 2010.

[2] Tamer A. Kawady, Naema Mansour, Abdel-Maksoud Taalab, "Performance Evaluation of Conventional Protection Systems for Wind Farms", IEEE/PES General Meeting, GM-2008, Pittsburg, 20-24 July, 2008.

[3] A. G. Phadke and J. S. Thorp, "Computer Relaying for Power Systems", Second edition, New York: Wiley, 2009.

[4] C.-S.Yu, "A Reiterative DFT to Damp Decaying DC and Subsynchronous Frequency Components in Fault Current", IEEE Trans. on Power Delivery, vol. 21, no. 4, Oct. 2006, pp. 1862-1870.

[5] A. A. Girgis, W. B. Chang, and E. B. Makram, "A Digital Recursive Measurement Scheme for On-Line Tracking of Power System Harmonics" IEEE Trans. Power Delivery, vol. 6, no. 3, July 1991, pp. 1153-1160.

[6] A. A. Girgis, and E. B. Makram, "Application of Adaptive Kalman Filtering in Fault Classification, Distance Protection, and Fault Location Using Microprocessors" IEEE Trans. on Power Systems, vol. 3, no. 1, Feb. 1988, pp. 301-309.

[7] Y. V. Murty and W. J. Smolinski "A Kalman Filter Based Digital Percentage Differential and Ground Fault Relay for a 3-phase Power Transformer" IEEE Trans. on Power Delivery, vol. 5, no. 3, July 1990, pp. 1299-1308.

[8] A. A. Girgis, W. B. Chang, and E. B. Makram, "Analysis of High-Impedance Fault Generated Signal Using A Kalman Filtering Approach," IEEE Trans. Power Delivery, vol. 5, no. 4, Nov. 1990, pp. 1714-1724.

[9] M. S. Sachdev and M. Nagpal, "A recursive least error squares algorithm for power system relaying and measurement applications", IEEE Trans. on Power Delivery, vol. 6, no. 3, Jul. 199, pp. 1008–1015.

[10] E. Rosołowski, J. Iz´ykowski, and B. Kasztenny, "Adaptive measuring algorithm suppressing a decaying dc component for digital protective relays", Electric Power System Research Journal, Elsevier, vol. 60, 2001, pp. 99–105.

[11] Y. Guo,M.Kezunovic, and D. Chen, "Simplified Algorithms for Removal of the Effect of Exponentially Decaying dc-Offset on the Fourier Algorithm", IEEE Trans. on Power Delivery, vol. 18, no. 3, Jul. 2003, pp. 711–717.

[12] D. Hornak, N. Chau, "Green power - wind generated protection and control considerations", Protective Relay Engineers, 2004 57th Annual Conference for, 30 Mar-1 Apr 2004, pp. 110 – 131.

[13] S. Haslam, P. Crossley and N. Jenkins, "Design and evaluation of a wind farm protection relay", Generation, Transmission and Distribution, IEE Proceedings, vol. 146, no. 1, Jan. 1999, pp. 37 – 44.

[14] Stefan Bauschke1, Clemens Obkircher, Georg Achleitner, Lothar Fickert and Manfred Sakulin, "Improved Protection system for electrical components in wind energy plants", 15th International Conference on Power System Protection, PSP '2006, Bled-Slovenia, 6-8 Sept. 2006.

[15] Tamer kawady, Naema Mansour and Abd El-Maksoud I. Taalab, "Evaluating the Role of Current Limiting Fuses for Wind Farm Protection Applications", IEEE-PES General Meeting-2009, Calgary, Canada, 26-30 July, 2009.

[16] Tamer Kawady, "An Interactive Simulation of Grid-Connected DFIG Units for Protective Relaying Studies", IEEE PES/IAS Sustainable Alternative Energy Conference-2009, Valencia-Spain, 28-30 Sept., 2009.

[17] Y. N. Chang, Y. C. Hsieh and C. S. Moo "Truncation Effects on Estimation of Dynamic Harmonics in Power System", International Conference on Power System Technology, PowerCon 2000, pp. 1155 – 1160, 4-7 Dec. 2000, Australia.

[18] C. S. Moo, Y. N. Chang and P. P. Mok "A Digital Measurement Scheme for Time-Varying Transient Harmonics", IEEE Trans. on Power Delivery, vol. 10, no. 2, April 1995.

[19] A.G. Phadke and J.S. Thorp, "Synchronized Phasor Measurements and Their Applications", Springer, New York, USA, 2008.

[20] J. Warichet, T. Sezi, J.-C. Maun, "Considerations about synchrophasors measurement in dynamic system conditions", Electrical Power and Energy Systems, vol. 31, 2009, pp. 452-464.